ISSN (Print) 1226-1750
ISSN (Online) 2233-6656
Journal of Magnetics 25(2), 233-244 (2020) https://doi.org/10.4283/JMAG.2020.25.2.233

Look-up Data Tables-Based Modeling of Switched Reluctance Machine and Experimental Validation of the Static Torque with Statistical Analysis

Ali Asghar Memon[1], Muhammad Mujtaba Shaikh[2], Syed Sabir Hussain Bukhari[3,4], and Jong-Suk Ro[4*]

[1]*Department of Electrical Engineering, Mehran University of Engineering and Technology, Jamshoro, Sindh, Pakistan*
[2]*Department of Basic Science and Related Studies, Mehran University of Engineering and Technology, Jamshoro, Sindh, Pakistan*
[3]*Department of Electrical Engineering, Sukkur IBA University, Sukkur, Sindh, Pakistan*
[4]*School of Electrical and Electronics Engineering, Chung-Ang University, Seoul, Korea*

(Received 5 April 2020, Received in final form 19 June 2020, Accepted 22 June 2020)

The look-up data-based modeling of switched reluctance machine and the procedure of validation of experimentally obtained static torque with statistical analysis is presented in this paper. First, the experimental setup for data collection of flux linkage and static torque is established and data is collected at an unequally spaced current and rotor position so that computation of instantaneous phase current and torque can be achieved. Second, the experimental data of static torque is compared with computed data. The computation is done in MATLAB software. Third, for numerical simulations, finite difference approximations and numerical integration schemes are used to compute co-energy and static torque profiles, respectively. The comparison is carried out in terms of different statistical parameters, including absolute and relative error distributions of the measured and computed torque profiles. A correlational study, to observe the extent to which both profiles exhibit a similar trend is also carried out. Finally, the influence of computed torque is carefully analyzed by running machine in single pulse mode and current chopping mode separately. The comparison with experimental data and the statistical analysis of results show the time efficiency, accuracy, and validity of the numerically simulated torque profiles.

Keywords : Flux linkage, mathematical modeling, numerical integration switched reluctance motor, static torque, statistical analysis

1. Introduction

The attraction of a switched reluctance (SR) machine is due to its simplicity, performance, and high starting torque. The simplicity of the machine reveals from its construction as windings are found on stator only. The phase arrangement is distinctive if compared with induction and DC motors. Therefore, SR motor is available in different phase arrangements such as 2-phase, 4-phase, 6-phase, etc. The addition of phases may have advantages and disadvantages, such as less or more torque ripple and additional losses due to the number of additional electronic devices used in the converter of the machine and copper used in the phase windings. Figure 1 shows one phase connections of an 8/6-pole machine. The energy flow and converter operation for a single-phase can be explained as when electronic switches T1 and T2 are closed, electrical energy is supplied to motor windings under +Vs (magnetization). When T2 is closed and T1 is opened, energy freewheels (Freewheeling) under Vs = 0 V, and when T1 and T2 are opened, energy is partly returned back to the source due to −Vs (de-magnetization) [1]. When stator phase windings are energized, the magnetic pull of the stator pole attracts the nearest unexcited rotor pole, resulting in increased inductance and decreased reluctance region. Similarly, when the next pole is energized, the previous rotor pole departs away from the attraction. In this case, inductance decreases, and reluctance increases.

In the past, several studies were devoted to examining the static characteristics of switched reluctance (SR) machines using mathematical modeling approaches and experiments carried out on an existing machine. The numerically simulated results obtained by solving mathematical models of SR machines are often verified using measured experimental data of the machines. The speed

©The Korean Magnetics Society. All rights reserved.
*Corresponding author: Tel: +82-2-820-5557
Fax: +82-2-820-5557, e-mail: jongsukro@gmail.com

© 2020 Journal of Magnetics

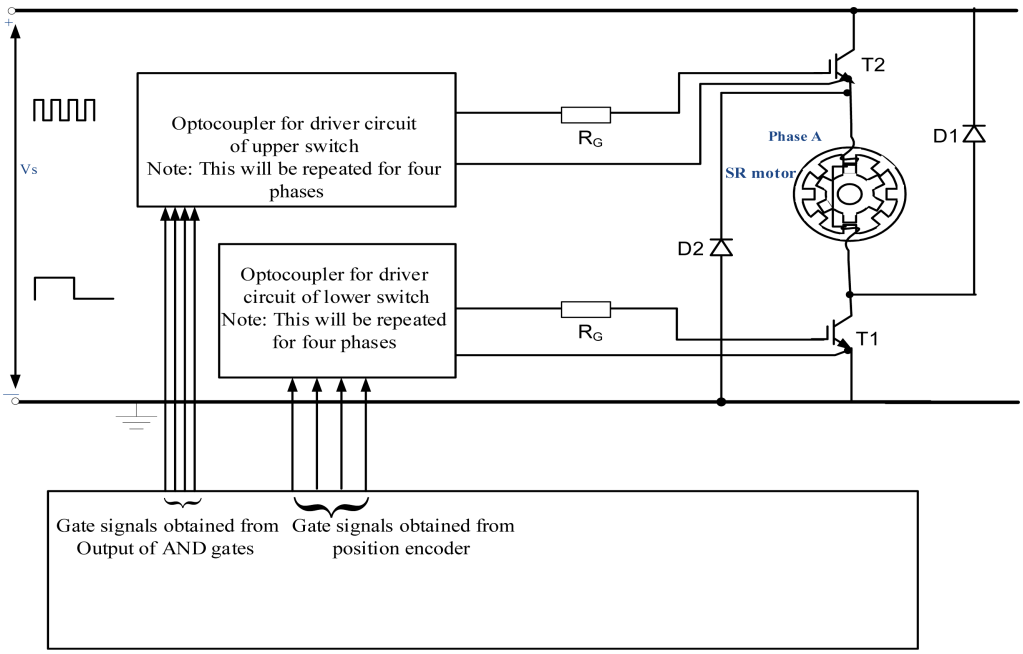

Fig. 1. (Color online) One phase connection and control circuits of 8/6-pole switched reluctance motor.

control and reduction in torque ripple in SR machines were the main objectives in past studies. Besides, new and efficient models for accurate profiling of SR machines were also discussed.

Jebarani, Kumar and Jayakumar [2] introduced a non-parametric model based on the least-squares' support vector machine coupled with optimal selection by differential Evolution to model the torque precisely and accurately in SR motor. The model was implemented using the finite element (FE) method on the magnetic characteristics of a motor. The results were also compared with similar optimal selection using genetic algorithm and particle swarm optimization. In reference [3], Ganji and Askari used an ANSYS package for 2-D transient analysis of the electromagnetic simulation model based on FE analysis. Meanwhile, the authors also discussed the characteristics of the conventional SR motors with new topologies, referred as segmental translator linear SR motor. The consequent properties of conventional and new SR motors were analyzed. Faiz and Finch [4] designed a package for a multiple teeth SR motor for improved performance based on the assumed flux path method. Also compared the results with measured values and those by the FE method. Li and Cho [5] proposed a method to minimize the unbalanced magnetic force and resulting vibrations caused due to rotor eccentricity in SR motors by using the parallel path windings. Transient FE analysis in two dimensions was carried out with different serial and parallel connections and it was demonstrated that for balance currents, parallel paths should be preferred which also allows the reduction in unbalanced magnetic force. The simulation results were also verified in the context of experimental results.

Arias, Rain, and Hilairet [6] used a stator flux estimation-based method and achieved improved estimations to stator flux and angle were achieved for SR machines by using some sensorless controllers. The actual voltage is maintained even at low-speed regimes, and the results were compared with experimental ones for various load and low-speed operations of the machine. Rafael, Branco, and Pires [7] introduced sliding mode controllers to control angular positions in SR machines which were based on machine torque characteristics. The underlying technique was applied on a 4-phase 8/6-pole SR machine and results were validated using experimental data. The proposed system was claimed to be low-cost and hence can attract the market. Tursini *et al.* [8] described a five-phase SR motor design for medium size aircraft which satisfied the consequent load requirements. Using the FE study, a thorough study of faulty and healthy motor performance was investigated, and static characteristics were discussed and compared to those obtained using experiments.

Dehkordi *et al.* [9] developed a new intelligent controller based on brain emotional learning for speed control of SR machines and compared its performance with the fuzzy logic controller. The preference of the proposed controller was demonstrated under different operating conditions and thus a new protocol was suggested for better estimation

of the rotor position using the ANFIS technique. Saha and Panda [10] used a hybrid many optimizing liaison gravitational search algorithm in outer and inner loops for speed control and reduction in torque ripples of 60 kW, 3-phase 6/8-pole SR motor. The results were compared with those obtained using the gravitational search algorithm (GSA). Significant reduction in torque ripple coefficient, integrated square errors (ISEs) of current and speed were achieved. Saha, Panda, and Panda [11] with similar objectives, as in [10], discussed speed control and reduction in torque ripple by using the many optimizing liaison (MOL) method and compared the results with those obtained by GSA. Marcsa and Kuczmann [12] attempted to reduce unnecessary torque ripple in a 3-phase 6/4-pole SR motor using geometry update and control strategy. Three-dimensional FE simulations were used for determining the skewing angle and the conventional performance was compared with enhanced performance and the proposed strategy was proved to be effective.

Kalaivani, Subburaj, and Iruthayarajan [13] framed the problem of speed control in an SR motor with the reduction in torque ripples as a multi-objective optimization problem to minimize the integral squared error in torque ripple and speed. The mechanism included outer and inner proportional-integral controllers for speed and current respectively and also the turn off angles for 3-phase 6/4-pole SR motor. The superiority of a non-dominated sorting genetic algorithm was shown for the optimal solution versus real coded genetic algorithm with simulated binary crossover. Abootorabi, Markadeh, and Soltani [14] used an input-output feedback linearization technique with nonlinear speed tracking and other control strategies on a 3-phase synchronous reluctance motor to regularize the stator flux and direct torque. Results were validated using simulation and experiments. Rain, Hilairet, and Arias [15] proposed two alternatives, a software and a hardware-based, by regulating sampling frequency while maintaining average torque and torque ripple stability and SR motor performance. While both alternatives were successful in reducing torque ripples by almost 45 % as compared to the original average torque control, the software-based alternative was completely cost-free. Ganji, Mansourkiaee, and Faiz [16] developed a high speed and accurate core loss model to design the optimal characteristic of the SR machine discussed its suitability over a previous core model using the finite element method (FEM). For MATLAB implementation of the proposed core loss model, only the design and control parameters were needed. The implementation of the model was discussed for 8/6-pole SRM and validated using experimental data and computation results of FEM.

In [17], static and dynamic models for the machine air gap were addressed and an analytical solution based on the Laplace equation and FEM was introduced. The results were obtained from the proposed uniform part of the air gap model. The factors affecting current waveforms were produced and discussed [18] by numerical simulation using the finite element time-stepping analysis method. In [19, 20], some analytical methods were promoted for computation of inductance of switched reluctance machine, and results were compared with those obtained from experiments. However, for nonlinear models, a fully analytical solution is mostly very difficult to attain, nevertheless, a desirable amount of accuracy and precision can be achieved with approximations. In [21], the authors proposed a dynamic circuit model, the magnetic circuit is represented into several individual magnetic circuit components which are dealt with separately. Only phase current waveforms were shown. Transient FEA and their proposed circuit model were used for the numerical simulation of air gap torque of switched reluctance machine. The main focus was made on core losses in [21], likewise in [22] on convertor losses in SRM.

In this study, we attempt to obtain static characteristics of the torque profile of the SR machines using numerical techniques. The experimental data tables of flux linkage and inverted flux linkage are used to compute co-energy using numerical integrations scheme, which finally leads to compute the static torque profile of the machine using finite difference approximation. The computed torque profile obtained using numerical simulation in MATLAB software is compared with the measured torque profile obtained through experiments conducted on an existing 8/6-pole, 4-phase SR machine. To measure the accuracy of computed torque profile and for its experimental validation, the statistical analysis of the results is carried out in terms of absolute and relative error (maximal positive, maximal negative and mean) distributions in computed torque profile with reference to the measured profile. The trend of both torque profiles is analyzed using a correlation study at different values of current. The accuracy of the computed torque profiles for an SR machine is demonstrated in terms of the statistical parameters. The comparison with experimental results is also carried out.

2. Materials and Methods

2.1. Simulation model of Switched Reluctance Machine

To determine the phase current i, of the SR motor, the basic simulation model used by many researchers [23-28] is the following equation:

$$v = Ri + \frac{d\psi}{dt} \tag{1}$$

where v is the applied voltage, R is the winding resistance, and ψ is the flux linkage.

Using a basic relationship between the flux linkage and current, i.e.

$$\psi = Li \tag{2}$$

Equation (1) can be expressed as

$$v = Ri + L\frac{di}{dt} + i\frac{dL}{dt} \tag{3}$$

If θ is the rotor position then, using chain rule in equation (3),

$$v = Ri + L\frac{di}{dt} + i\frac{dL}{d\theta}\omega \tag{4}$$

where $\omega = d\theta/dt$ is the angular speed rad/sec.

where, the applied voltage is expressed as the sum of the resistive voltage drop, inductive voltage drop, and the induced EMF, respectively. To see the breakup of total power, vi, multiplying equation (4) by phase current i, leads to:

$$vi = Ri^2 + \frac{d}{dt}\left(\frac{Li^2}{2}\right) + i^2\frac{dL}{d\theta}\omega \tag{5}$$

Equation (5) shows that the total power is the sum of power loss, rate of increase of stored magnetic energy, and power converted from electrical energy to mechanical output power, respectively.

The Electromagnetic torque of SRM is given by equation (6).

$$T = i^2\frac{dL}{d\theta} \tag{6}$$

For dynamic characteristics of SRM, a mechanical equation (7) is added,

$$\frac{d\omega}{d\theta} = \frac{1}{J}(T - T_L) \tag{7}$$

where w is used for rotational speed, T is used for the torque of the machine, T_L represents load torque, and J denotes the moment of inertia.

2.2. Static Characteristics of Switched Reluctance Machines

To accomplish the best simulation model of switched reluctance motor based on the look-up data tables, it is perceptible that data tables of flux linkage $\psi(\theta, i)$, co-energy $W'(\theta, i)$ and static torque characteristics $T(\theta, i)$, respectively are required for simulation [23]. These characteristics are much reliant on current and rotor positions of the machine [24, 25]. As far as the measurement of flux linkage characteristics pen name magnetizing characteristics is concerned different methods of measurement are documented in literature such as search coil method [26] and an integrator circuit [25]. Simulation technique is another way of getting these characteristics through computer programming [27-34].

2.3. Basic Relations

Once the data of induced E. M. F across the machine winding is available, the flux linkage ψ can be obtained using the relationship:

$$\int EMFdt = \psi \tag{8}$$

Having obtained flux linkage from (8), the relationship (2) can be used to calculate the inductance profile of the machine.

The co-energy W' and the flux profiles of the SR machine depending on current measurements i and the position θ are related by equation (9):

$$W'(\theta, i) = \int_0^i \psi(\theta, u)du \tag{9}$$

Co-energy profile from equation (9) can be utilized for the computation of static torque $T(\theta, i)$ of the machine as described in equation (10):

$$T(\theta, i) = \frac{\partial W'(\theta, i)}{\partial\theta} \tag{10}$$

3. Experimental Data

Inspired by the technique presented in [35-46], the data of induced EMF in the search coil of an existing switched reluctance prototype (shown in Fig. 2(a)). Fig. 2(b) shows pole structure and Fig. 2(c) represents the asymmetrical converter with 4-phase connections of SRM. This data of E.M.F (shown in Fig. 3) was needed to obtain flux by equation (8). Figure 3 represents the aligned position, where inductance is maximum and reluctance is minimum. Similarly, Fig. 4 highlights the unaligned position of the machine poles where inductance is minimum and reluctance is maximum. For accurate modeling and reliable performance of the machine, it is required to have a trend of obtained results as similar to the experimental. The computer graphical environment of software, named Lab VIEW (Laboratory Virtual Instrumentation Engineering Workbench) has been used to accumulate the required data of flux. For this setup SR machine: D-80, 0.75 kW,

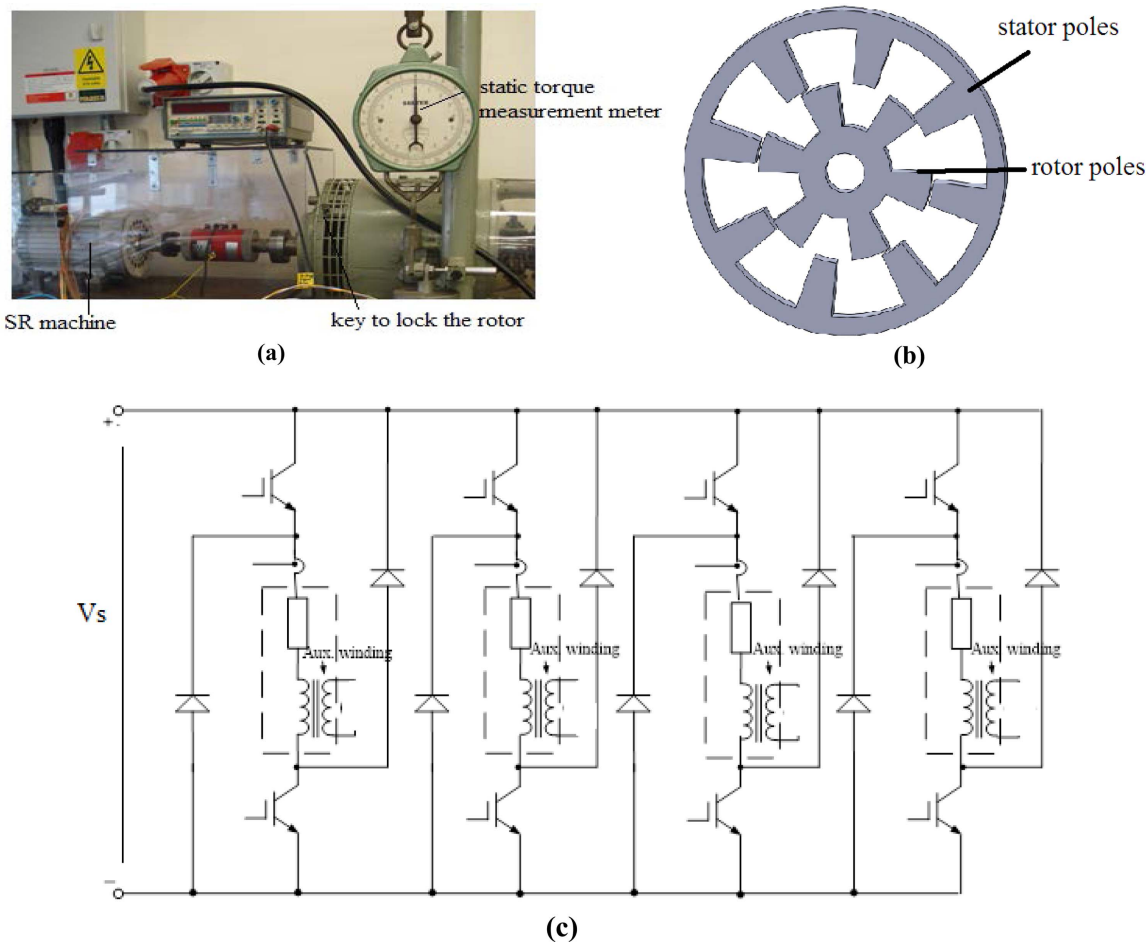

Fig. 2. (Color online) (a) Experimental setup for measurement of static torque data, (b) 8/6 - pole structure of SRM, and (c) Asymmetrical converter and 4-phase connections of SRM.

and 1500 rpm are used. Figure 3 describes the flux linkage characteristics for different currents and rotor positions. Figure 5(a) shows a set of measured flux linkage characteristics. Figure 5(b) shows a set of flux linkage characteristics in a 3-D view. However, the flux distribution at aligned and unaligned positions is shown in Fig. 5(c).

Using a locked rotor test and by allowing the current to flow through the motor winding, the experimental data of static torque was measured using a dynamometer (Fig. 2). This experimental data has been used to plot the static torque characteristics. These characteristics are shown in the forthcoming section. Since the accuracy of the torque transducer was not good due to noise, despite a capacitor of 200 nF was introduced at the output. Another reason for using spring balance attended with a load dynamometer for the measurement of torque compared with toque transducer was its poor stability between ranges of speed from 300-400 rpm. The accuracy of the dynamometer was found up to 10 Nm.

4. Numerical Simulation for the Computation of Static Torque

The data of static torque described in [35, 36] and Table 1 will be used in the forthcoming sections to validate the results for the computed torque using numerical simulations.

Using the data of flux linkages, the static torque can be computed using numerical integration on $\psi(\theta, i)$ followed by numerical differentiation of $W'(\theta, i)$. The process is described here in detail.

Let i_k (k = 0, 1,.., n) be the (n + 1) currents, and $\psi(\theta_i, i_k)$ be the corresponding flux linkages across some fixed positions θ_j (j = 1, 2,.., m), the co-energy profile from equation (7) can be obtained by numerical integration of $\psi(\theta, i)$ with respect to the current i. For this purpose, a closed Newton-Cotes quadrature approximation [37, 38] with p nodes, $Q(p)$ can be used, and for a fixed j, it is defined as:

$$W'(\theta_j, i_k) \approx Q_{(p)}\left[\psi(\theta_j, i_k)\right] = \sum_{r=0}^{p-1} c_r h^{r+1} S_{p,r} \tag{11}$$

Table 1. Measured static torque of the machine.

Specified current [A]	Position [deg.]	Measured static torque [Nm]
	0	0
2	–6	0.75
	–12	0.8
	0	0
5	–9.25	3.8
	–15	4.2
	0	0
6	–7	4.1
	–15	5.45
	0	0
10	–9	8.65
	–12	10

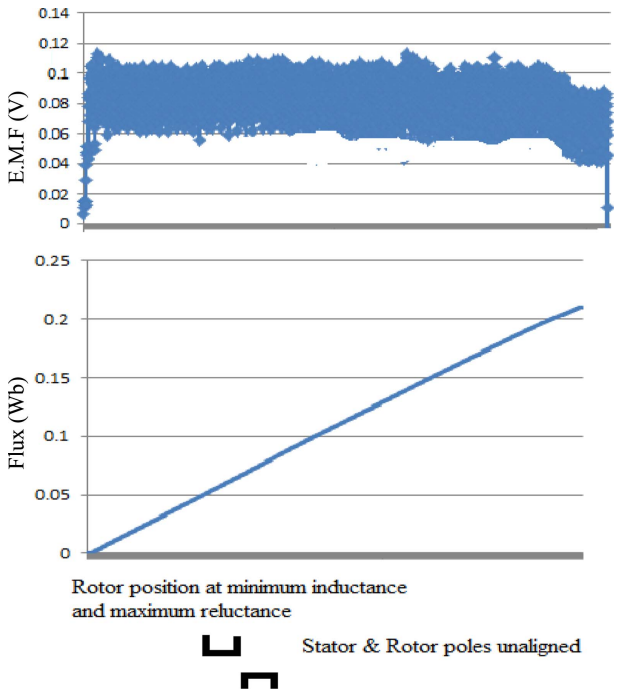

Fig. 3. (Color online) Experimental data of E.M.F and computationally obtained Flux waveform of the machine at the unaligned position.

$$c_r = \frac{\Delta^r \psi(\theta_j, i_0)}{h^r . r!},\ r = 0, 1, .., p-1 \text{ and } h = \frac{i_k - i_0}{n}, \tag{12}$$

$$S_{p,r} = \begin{cases} \int_0^{p-1} dt & , r = 0 \\ \int_0^{p-1} \prod_{q=0}^{r-1} (q-r)\, dt & , r \geq 1 \end{cases} \tag{13}$$

and

$$\Delta^r \psi(\theta_j, i_0) = \sum_{q=0}^{r} (-1)^r C_q^r \psi(\theta_j, i_{r-q}),\ r = 0, 1, ..., p-1 \tag{14}$$

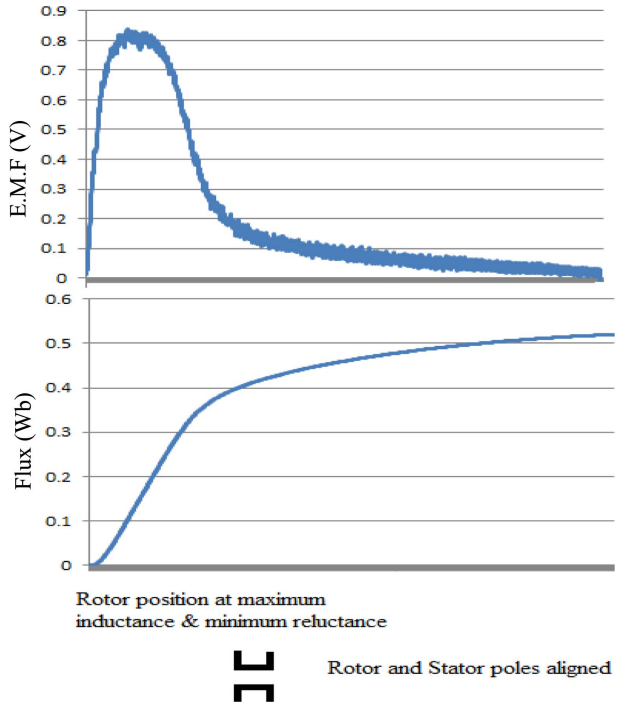

Fig. 4. (Color online) Experimental data of E.M.F and computationally obtained Flux waveform of the machine at the aligned position.

For the estimation purpose in this study, we use the well-known trapezoidal approximation of the integration in (9), and its variants were successfully used in [39] for solving Fredholm integral equations of the second kind and in [40] for evaluating Riemann-Stieltjes integrals numerically. The trapezoidal approximation for the co-energy in terms of the flux linkage data can be obtained by setting $p = 2$ in equations (11)-(14). Once the co-energy profiles are computed for all currents, shown in Fig. 6, equation (8) can then be used with numerical differentiation on the co-energy profiles to compute the numerical torque profiles, shown in Figs. 7-9. Using a finite difference approximation of the partial derivatives of $W'(\theta, i)$ with respect to the position at a fixed current i_k in (10), we obtain the computed static torque profiles as follows:

$$T(\theta_j, i_k) = \frac{\partial}{\partial \theta}\left[W'(\theta_j, i_k)\right] \approx \frac{W'(\theta_{j+1}, i_k) - W'(\theta_j, i_k)}{\theta_{j+1} - \theta_j},\ j = 1, 2, ..., m \tag{15}$$

5. Parameters Used for Statistical Analysis

For sensitivity analysis of the numerically computed static torque profiles with reference to the experimentally measured data of static torque, we use various statistical

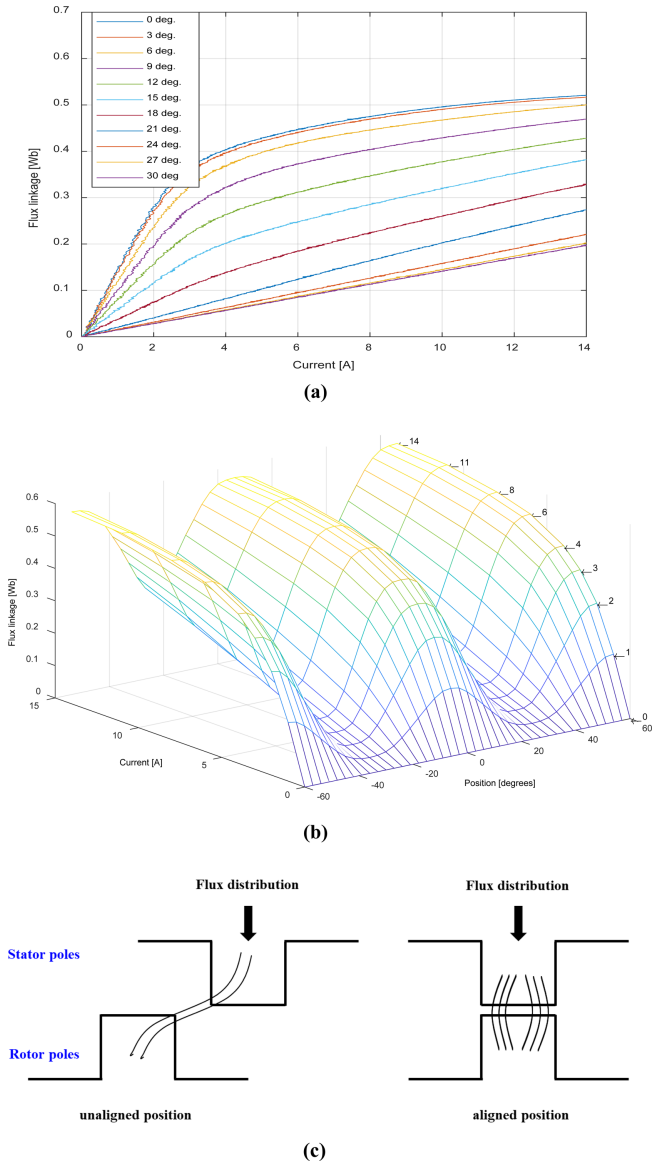

Fig. 5. (Color online) (a) Flux linkage characteristics, (b) Flux linkage characteristics (3-D illustrations), (c) Flux distribution at aligned and unaligned position.

parameters to compute error distributions and correlation parameters between both profiles in the next sections. Let i_k be some specified current, $MT(\theta_i, i_k)$ and $CT(\theta_i, i_k)$ denote the measured and computed torque profiles comprising of m-nodes with respect to the positions θ_j, j = 1, 2,…m, respectively, then the mean measured torque and the mean computed torque at some i_k can be obtained by using equations (16) and (17), respectively.

$$\mu_{MT}(i_k) = \frac{\sum_{j=1}^{j=m} MT(\theta_j, i_k),}{m} \quad k = 0,1,\ldots,n \tag{16}$$

$$\mu_{CT}(i_k) = \frac{\sum_{j=1}^{j=m} CT(\theta_j, i_k),}{m} \quad k = 0,1,\ldots,n \tag{17}$$

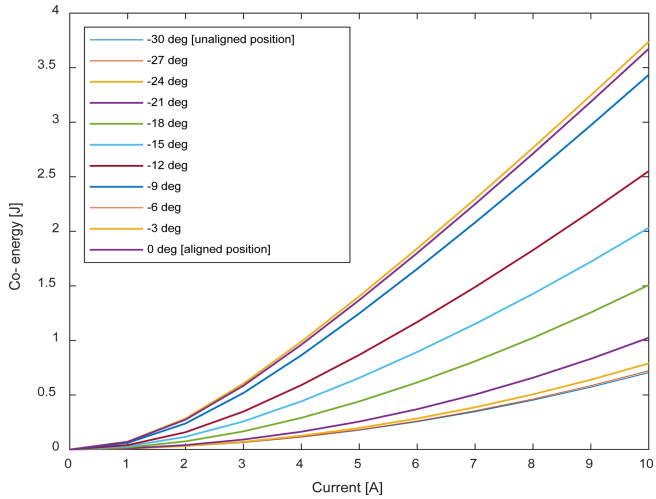

Fig. 6. (Color online) Numerically computed co-energy waveforms versus current.

5.1. Error distributions

To see the discrepancy in the measured and computed static torque profiles, at some specified current i_k, the absolute error distributions across all positions θ_j can be computed using (18) [41, 42]:

$$\left|\varepsilon_{i_k}\right| = \left|MT(\theta_j, i_k) - CT(\theta_j, i_k)\right|, \quad \text{for all } j, \text{ and } k = 0,1,\ldots n \tag{18}$$

The maximal positive and negative relative errors [41-42] across all positions, at some specified current i_k, can be computed as:

$$R.E_{i_k}^{+} = \max_{\forall j}\left|\frac{MT(\theta_j, i_k) - CT(\theta_j, i_k)}{MT(\theta_j, i_k)}\right|, \; k = 0,1,\ldots n \tag{19}$$

$$R.E_{i_k}^{-} = \max_{\forall j}\left|\frac{CT(\theta_j, i_k) - MT(\theta_j, i_k)}{MT(\theta_j, i_k)}\right|, \; k = 0,1,\ldots n \tag{20}$$

Equation (19), for a fixed current, determines the magnitude of the largest possible difference by which the computed static torque is lower than the measured static torque across all positions at that current. On the other hand, the magnitude of the largest possible difference, across all positions at a specified current, by which the computed torque is higher than the measured torque, can be found using equation (20).

5.2. Correlation analysis

It is also important to examine whether the numerically computed torque profiles exhibit a similar trend as of the measured torque profiles. To see the direction and strength of the relationship of both static torque profiles, a correlation study is conducted in terms of two well-

known formulas appearing in the literature [41-44]. For a fixed current i_k, the correlation formulas between the measured and computed torque profiles with respect to all positions, take the form:

$$r_{i_k} = \frac{m\sum_{j=1}^{j=m}\left[MT(\theta_j,i_k).CT(\theta_j,i_k)\right] - \sum_{j=1}^{j=m}MT(\theta_j,i_k).\sum_{j=1}^{j=m}CT(\theta_j,i_k)}{\sqrt{\left[m\sum_{j=1}^{j=m}\left\{MT(\theta_j,i_k)\right\}^2 - \left\{\sum_{j=1}^{j=m}CT(\theta_j,i_k)\right\}^2\right]\left[m\sum_{j=1}^{j=m}\left\{CT(\theta_j,i_k)\right\}^2 - \left\{\sum_{j=1}^{j=m}MT(\theta_j,i_k)\right\}^2\right]}}, \quad k = 0,2,\ldots,n \tag{21}$$

$$\Theta_{i_k} = \sqrt{1 - \frac{\sum_{j=1}^{j=m}\left[MT(\theta_j,i_k) - CT(\theta_j,i_k)\right]^2}{\sum_{j=1}^{j=m}\left[MT(\theta_j,i_k) - \mu_{MT}(i_k)\right]^2}}, \quad k = 0,1,\ldots,m \tag{22}$$

where r_{i_k} and Θ_{i_k} are the coefficient of correlation and correlation quotient between experimentally measured and numerically computed static torque profiles, respectively. Generally, the correlation constants in equations (21) and (22) vary in the range –1 to 1. A computed torque profile for some fixed current i_k, for which the correlation constant is closer to +1 is considered to have a more similar trend to that of the measured torque profile at the same current. The ideal case, i.e. the perfect positive correlation is experienced when the correlation constants are equal to +1. Equations (21) and (22) are also efficient ways of comparing the computed and measured torque profiles.

6. Results and Discussions

Using equations (11)-(15) with $p = 2$ to numerically integrate the flux profiles with respect to the current nodes co-energy waveforms were computed. The computed torque curves are produced in MATLAB software, are shown in Fig. 7 corresponding to the positions –30° to 30° for various constant currents 0-14A. For better understanding and testing of the computed static torque profiles, we repeated the simulations using equations (11)-(15) with extended values for position and current, particularly for positions ranging from –60° to 60° and currents ranging from 0A to 20A. The results of the extended simulation are shown in Fig. 8. For the experimental verification, the experimentally measured values of static torque and the numerically computed torque profiles are shown together versus positions –30° to 0° in Fig. 9. More nodes for current can be added easily in the simulations. It can be observed from Fig. 9 that there is not much difference in the results between numerical simulation and experiment.

Figure 10 shows the mean static torque by simulation

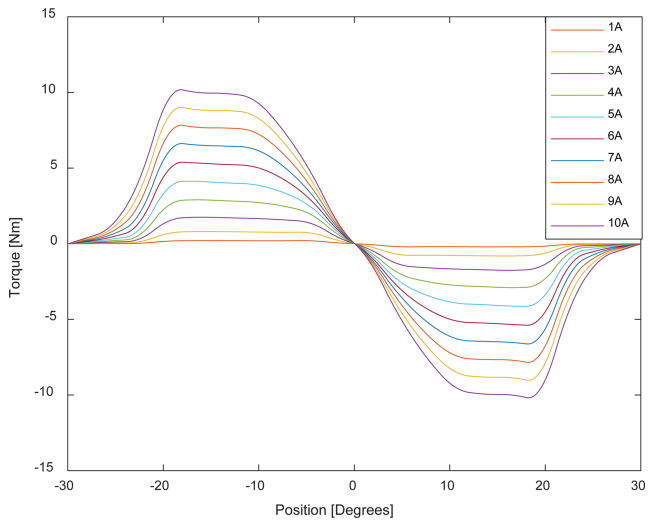

Fig. 7. (Color online) Computed static torque profiles versus position for constant currents ranging from 0 to 14A.

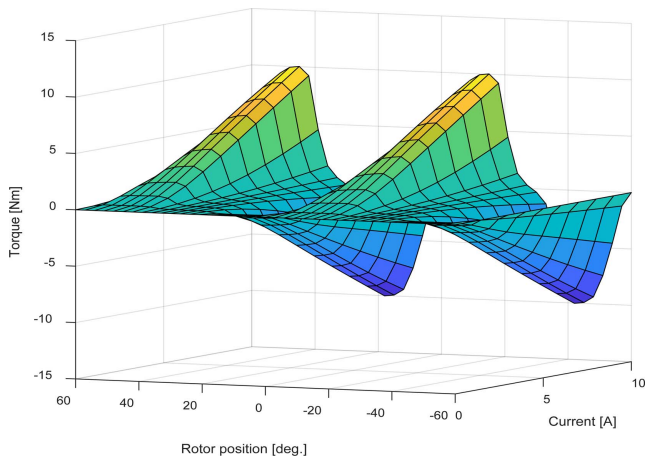

Fig. 8. (Color online) Computed torque profile.

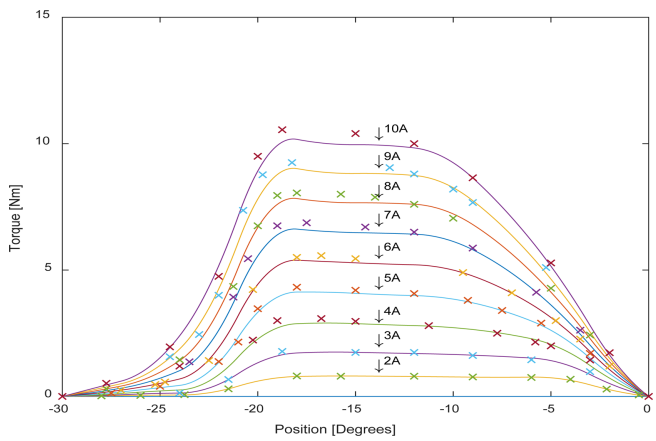

Fig. 9. (Color online) Static torque characteristics, 'x' for the measured torque and '...' for the computed torque.

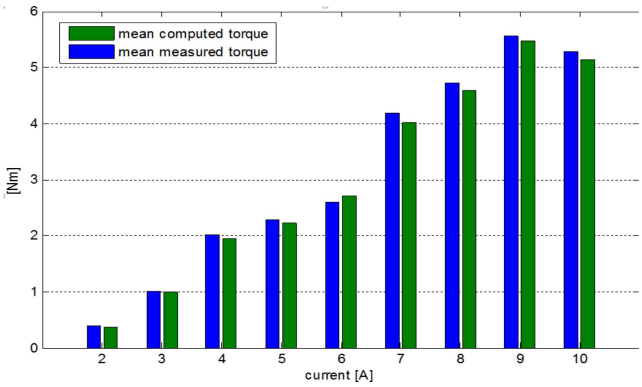

Fig. 10. (Color online) Mean computed and measured torques at constant currents.

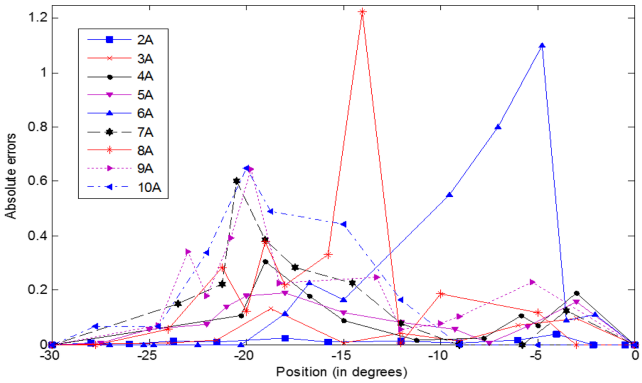

Fig. 11. (Color online) Absolute error distributions between computed and measured torque profiles.

and experimental approaches versus constant currents obtained using equations (16) and (17). The mean torque values do not exhibit considerable difference. For constant currents, the absolute error distributions in the numerically computed torque profiles with reference to the experimentally measured torque values at common points are described in Fig. 11 by using equation (18). It should be noted that equations (19) and (20) result in undefined values when the current is 0A due to zero denominators. For this reason, absolute error distributions were preferred over the relative error distributions for visualization in Fig. 9.

Using equations (19) and (20), the magnitude of maximum possible errors, at fixed currents, by which the computed torque is lower than and greater than the measured torque

Table 3. Operating conditions for simulation results.

Parameter	Value
Resistance	2.5 Ω
Number of rotor poles	6
Number of motor phases	4
Applied voltage	50 V
Transistor threshold voltage	0.7 V
Transistor V/I gradient	0.055 Ω
Number of transistors per phase	2
Diode threshold voltage	0.7 V
Diode V/I gradient	0.08 Ω
Number of diodes per phase	2
Static friction	0.08 Nm
coefficient of viscous friction	0.0005 Nm/rad/sec
Switch on angle	–30 degrees
Switch off angle	0 degrees
Speed	300 rpm
I_{max}	4A
I_{min}	3.5A
Duty cycle	0.25 %
fc	2000 Hz

was calculated and are shown in Table 2. The mean absolute errors in both torque profiles across all positions are also summarized in Table 3 at fixed currents. The error parameters described in Table 3 are considerably small showing that the simulated results agree with the experimental results. However, the upper bound of error is observed for a position at 6A and another position at 8A because the experimental data were unequally spaced. However, it is clear from Fig. 9 (node wise comparison of computed and measured torques specially at 6A and 8A), Fig. 10 mean torques (computed and measured comparison specially at 6A and 8A) and Fig. 12 (correlation indices at all nodes specially at 6A and 8A) that the computed and measured values match quite well at 6A and 8A relative to other nodes.

The correlation analysis has been conducted using equations (21) and (22), which are two widely used formulas from the literature [41-44]. Using equations (21) and (22) on the computed and measured torque data, the obtained correlation constants are shown as bars in Fig. 12. The horizontal line shows the perfect positive correlation borderline. The extent to which correlation constants

Table 2. Maximum positive relative, maximum negative relative and mean absolute errors.

	2A	3A	4A	5A	6A	7A	8A	9A	10A
$R.E^{+}$	0.2	0.0969	0.1326	0.1428	0.0925	0.1103	0.1552	0.0737	.1258
$R.E^{-}$	0.0750	0.0490	0.0498	0.0642	0.3667	0.0000	0.0648	0.1392	.0712
$\mu_{A.E.}$	0.0094	0.0384	0.0991	0.0805	0.2099	0.1723	0.2084	0.1975	.1844

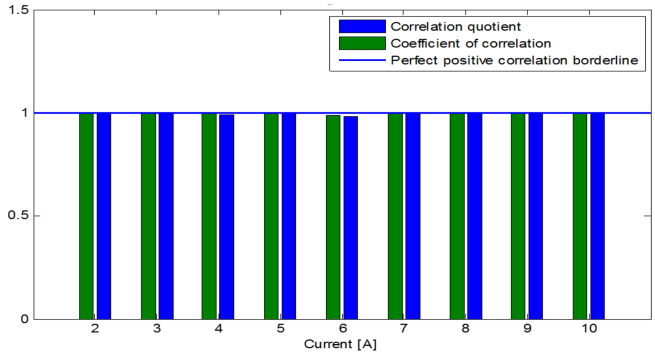

Fig. 12. (Color online) Correlation constant at constant currents and the perfect positive correlation borderline.

are closer to this borderline describes how likely it is to conclude the highest possible positive linear relationship between the variables. Observing Fig. 12, the correlation constants are mostly very close to +1, indicating a perfect positive correlation between the computed and measured torque profiles. Using Fig. 12, it can be safely concluded that the computed and measured torque data show a similar trend – with positive direction and almost 100 % strength – as the current values increase.

The reliability of simulation formulas used in this work and subsequent validation of simulation results by experimental data in form of graphs and statistical analysis show that the results obtained through numerical simulations can be accepted and are in agreement with the experimental results.

Numerical simulations of the machine have been obtained under the operating conditions described in Table 3. The complete simulation model of the SR machine based on the computed torque profiles and other data tables, discussed in previous sections in this study is shown in Figs. 13-15. Fig. 13 shows the instantaneous current, instantaneous torque, applied voltage, and flux during the operation of the machine under the single pulse mode. The waveform of current and torque is scaled by constant 4, whereas, flux by constant 30. It should be noted that once the experimental or simulated look-up data tables are available for EMF and flux linkage along with machine parameters, the simulations of the co-energy and static torque profiles presented here in this study can be obtained in much lower execution time. It required on average CPU time of 0.89 s with a standard deviation of 0.012 s to implement numerical integration schemes for co-energy

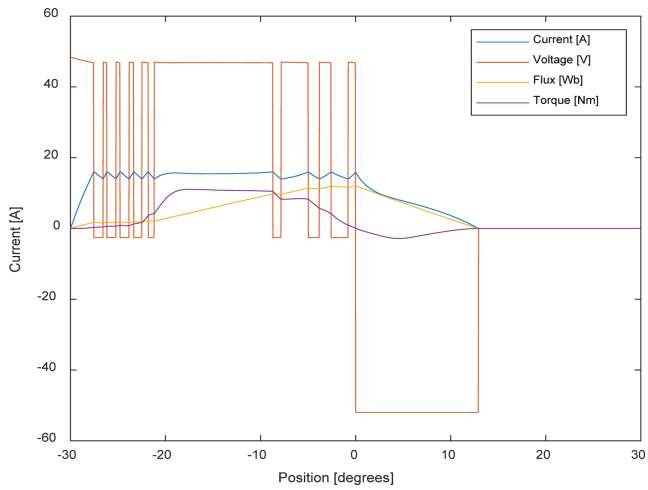

Fig. 14. (Color online) Instantaneous current, instantaneous torque, applied voltage, and flux waveforms (current chopping mode).

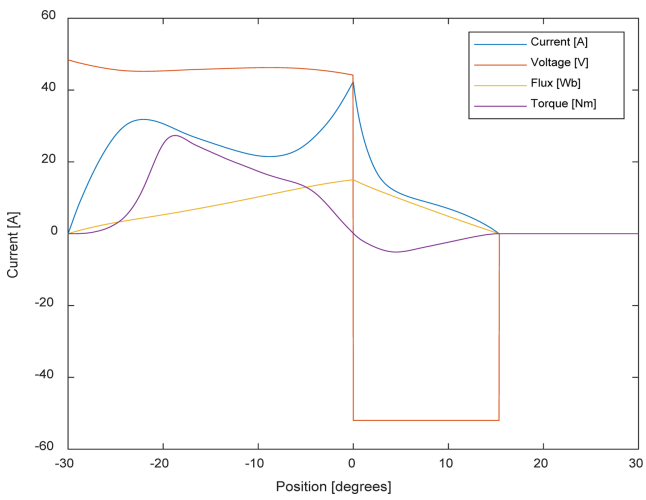

Fig. 13. (Color online) Instantaneous current, instantaneous torque, applied voltage, and flux waveforms (single pulse mode).

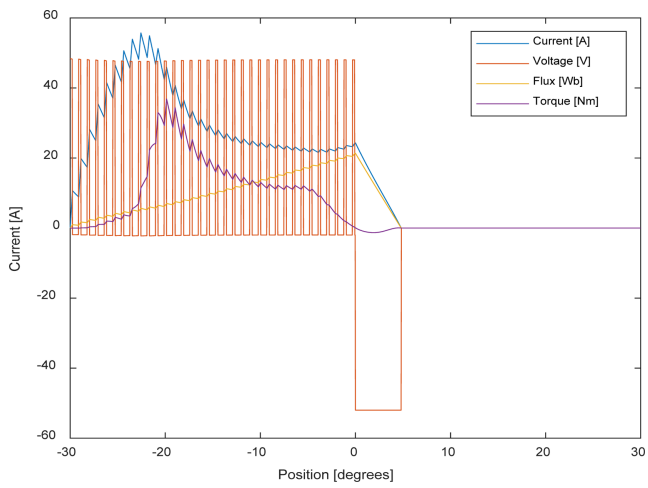

Fig. 15. (Color online) Instantaneous current, instantaneous torque, applied voltage, and flux waveforms (pulse width modulation mode).

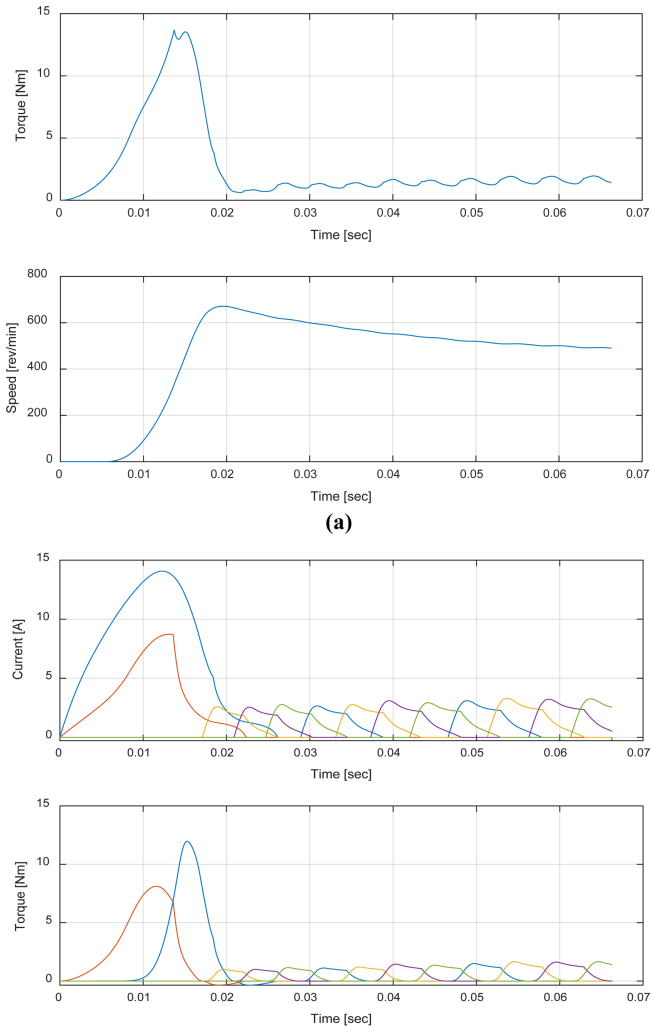

Fig. 16. (Color online) (a) Total torque of SRM, speed of SRM, (b) Instantaneous torque of 4-phases and Instantaneous current for 4-phase SRM (dynamic characteristics).

and finite difference approximations for the static torque on MATLAB software for consecutive 50 simulations.

Figure 14 shows the instantaneous current, instantaneous torque, applied voltage, and flux during the operation of the machine under the current chopping mode. The waveform of current and torque is scaled by constant 4, whereas, flux by constant 30. Figure 15 shows the instantaneous current, instantaneous torque, applied voltage, and flux during the operation of the machine under pulse width modulation mode. The waveform of current and torque is scaled by constants 50 and 70, whereas, flux by constant 150. Figure 16 is produced under dynamic operation of SRM, followed by operating conditions: R = 2.5W, switch on = −30 deg., switch off = −10 deg., J = 0.0012 kgm^2, load Torque = 1.83 Nm, V_s = 50 V.

In summary, the methodology of our study is based on an actual real SR motor look-up data tables. Thus, we used EMF, flux-linkage (see Figs. 2-5) data of the experimental motor and process it through numerical treatment/simulation using MATLAB software with numerical integration from equations (11)-(14) and finite difference scheme from equation (15) on the associated mathematical model so that co-energy and torque profiles (Figs. 6-8) can be computed with a good margin of accuracy (Fig. 9). Error and correlation analysis have also been carried out (Figs. 10-12 and Table 2). Finally, the computed torque profiles for current and positions have been successfully compared with real motor (Fig. 9) and comprehensively shown in Figs. 13-15.

7. Conclusions

The simulation model of the switched reluctance machine based on look-up data tables has been presented. The mathematical modeling using conventional equations was extended using numerical integration and finite difference schemes to successfully compute co-energy and static torque profiles of the machine, respectively. Experimentally measured data of the machine was used to check the accuracy of computed profiles using numerical simulations. The data of experimentally measured and numerically computed static torque profiles were compared exhaustively in terms of error and correlational analyses. The comparison based on different statistical parameters, comprising of absolute and relative error distributions of the measured and computed torque profiles were discussed. The comparison with experimental data and the statistical analysis of results have been found accurate and acceptable. The proposed simulation setup for the static torque and modeling of SRM with use of look-up data tables and the numerical algorithms is found to be time-efficient, valid, and accurate through exhaustive statistical analysis in comparison to other Simulink-based approaches in the literature.

Acknowledgement

This research was supported in part by Basic Science Research Program through the National Research Foundation of Korea funded by the Ministry of Education (2016R1D1A1B01008058), Human Resources Development (No. 20204030200090) of the Korea Institute of Energy Technology Evaluation and Planning (KETEP) grant funded by the Korea government Ministry of Trade, Industry and Energy, and by the Korea Research Fellowship Program through the National Research Foundation (NRF) of Korea funded by the Ministry of Science and

ICT (2019H1D3A1A01102988).

References

[1] P. J. Lawrenson, J. M. Stephenson, P. T. Blenkinsop, J. Corda, and N. N. Fulton, IEE Proceedings B Electric Power Applications (1980).
[2] E. S. Jebarani, S. S. Kumar, and J. Jayakumar, Neurocomputing (2016).
[3] B. Ganji and M. H. Askari, Alexandria Engineering Journal **55**, 3 (2016).
[4] J. Faiz and J. W. Finch, Computers & Electrical Engineering **20**, 3 (1994).
[5] J. Li and Y. Cho, Mathematics and Computers in Simulation **81**, 2 (2010).
[6] A. Arias, X. Rain, and M. Hilairet, Electric Power Systems Research 104 (2013).
[7] S. Rafael, P. C. Branco, and A. J. Pires, Electric Power Systems Research 129 (2015).
[8] M. Tursini, M. Villani, G. Fabri, and L. Di Leonardo, Electric Power Systems Research 142 (2017).
[9] B. M. Dehkordi, A. Parsapoor, M. Moallem, and C. Lucas, Energy Conversion and Management **52**, 1 (2011).
[10] N. Saha and S. Panda, Engineering Science and Technology, an International Journal **20**, 3 (2017).
[11] N. Saha, A. K. Panda, and S. Panda, Journal of Electrical Systems and Information Technology (2017).
[12] D. Marcsa and M. Kuczmann, Comput. Math. Appl. **74**, 1 (2017).
[13] L. Kalaivani, P. Subburaj, and M. W. Iruthayarajan, International Journal of Electrical Power & Energy Systems 53 (2013).
[14] H. A. Zarchi, G. R. A. Markadeh, and J. Soltani, Energy Conversion and Management **51**, 1 (2010).
[15] X. Rain, M. Hilairet, and A. Arias, Energy Conversion and Management 86 (2014).
[16] B. Ganji, Z. Mansourkiaee, and J. Faiz, Energy 89 (2015).
[17] A. Abdel-Razek, J. Coulomb, M. Feliachi, and J. Sabonnadiere, IEEE Trans. Magn. **18**, 2 (1982).
[18] M. J. Kamper, S. W. Rasmeni, and R-J. Wang, IEEE Trans. Magn. **43**, 7 (2007).
[19] D. Lin, P. Zhou, S. Stanton, and Z. J. Cendes, IEEE Trans. Magn. **4**5, 12 (2009).
[20] Zhang, Minjie, Qiang Gao, and Xu Cai, International Conference on Electrical Machines and Systems (2019).
[21] Yan, Wenju, Hao Chen, Kai Wang, and Lei Chen, IET Electric Power Applications **12**, 6 (2018).
[22] A. A. Memon, U. Yasir, and M. A. Uquali, International Conference on Electrical Machines and Systems (2017).
[23] J. M. Stephenson and J. Corda, IEE Proceeding **126**, 5 (1979).
[24] J. Corda and S. M. Jamil, IEEE Trans. Ind. Elect. **57**, 1 (2010).
[25] J. Corda, PhD thesis, University of Leeds 1979.
[26] Charles V. Jones, "The Unified Theory of Electrical Machines", London, 1967.
[27] A. D. Cheok and N. Ertugrul, IEEE Trans. Instrum. Meas. **50**, 3 (2001)
[28] H. Sahraoui, H. Zeroug, and H. A. Toliyat, IEEE Trans. Magn. **43**, 12 (2007)
[29] X.-D. Xue, K. W. E. Cheng, and S. L. Ho, IEEE Trans. Energy Conversion **17**, 4 (2002).
[30] S. Khotpanya, S. Kittiratsathca, and Ishi Kazuhisa, International Conference on Power Electronics and Drives Systems (2005).
[31] Wei Min Chan and W. F. Weldon, IEEE Industry Applications, Annual Meeting New Orleans, 1997.
[32] A. A. Memon, Syed Asif Ali Shah, Wajiha Shah, M. A. Baloch, G. S. Kaloi, and N. H. Mirjat, IEEE Access 6 (2018).
[33] Poorani Shivkumar, R. Murugan, and B. Sangeetha, Indian J. Sci. Technol. **8**, 11 (2015).
[34] E. Annie Elisabeth Jebaseeli, D. Susitra, and P. Abirami, Indian J. Sci. Technol. **8**, 28 (2015).
[35] A. A. Memon and M. M. Shaikh, Data in Brief 14 (2017).
[36] A. A. Memon, Ph.D Thesis, School of Electronics and Electrical engineering, University of Leeds, UK, 2012.
[37] C. C. Tseng, IEEE Transactions on Circuits and Systems I: Regular Papers **54**, 3 (2007).
[38] M. M. Shaikh, M. S. Chandio, and A. S. Soomro, Sindh University Research Journal-SURJ (Science Series) **48**, 2 (2016).
[39] M. M. Shaikh, Turkish Journal of Analysis and Number Theory **7**, 4 (2019).
[40] K. Memon, M. M. Shaikh, M. S. Chandio, and A. W. Shaikh, Sindh University Research Journal-SURJ (Science Series) **52**, 1 (2020).
[41] S. Genić, I. Aranđelović, P. Kolendić, M. Jarić, N. Budimir, and V. Genić, FME Transactions **39**, 2 (2011).
[42] M. M. Shaikh, S. U. R. Massan, and A. I. Wagan, Int. J. Heat Mass Transf. 88 (2015).
[43] R. E. Walpole, Introduction to statistics. Macmillan (1982).
[44] R. R. Wilcox, Basic statistics: understanding conventional methods and modern insights. Oxford University Press on Demand (2009).